Resonant inelastic charge transfer in short alanine bridges

Nikolai Sergueev and Alexander A. Demkov*
Department of Physics, The University of Texas at Austin, Austin, Texas 78712, USA
(Received 20 August 2009; published 11 January 2010)

We investigate theoretically the effect of atomic vibrations on the electron tunneling in polyalanine bridges. The inelastic-scattering processes in the bridge are included using a nonequilibrium Green's function formalism with the density-functional Hamiltonian. With this method we analyze the inelastic charge transfer in polyalanine. We find that electron tunneling across alanine exhibits a resonant behavior and that atomic vibrations substantially change the charge-transfer rate across the bridge by providing additional scattering channels.

DOI: 10.1103/PhysRevB.81.045112 PACS number(s): 72.10.−d, 81.07.Nb, 68.37.Ef, 73.63.−b

I. INTRODUCTION

Electrical conductivity of single organic molecules has been under intense study over the last decade. In molecular electronics single molecule systems have attracted substantial interest in view of their potential device applications.[1–6] At the same time, several biologically important processes such as photosynthesis,[7–10] aerobic metabolism,[11] or vision[12] involve electron transfer. Electrons travel across the biomolecule over distances as large as 30 Å. Understanding from the microscopic perspective how an electron travels through such a long distance is a very challenging yet important problem for theory.

A typical molecular electronics system consists of two macroscopic electrodes and a molecule (or molecules) bridging them. The functionality of such a device relies on the charge flow through the molecule and contact-molecule interfaces. Different experimental techniques including the mechanically controlled break junction[2,13,14] and scanning tunneling microscopy (STM) (Refs. 15–17) have been successfully used to measure the tunneling current and conductance of single molecule devices. Probing of the charge-transfer mechanism in the molecule is based here on a direct measurement of the molecular conductance. The electron transfer processes in biological complex molecules can also be studied via steady-state current measurements.[18–20] Indeed, measuring the steady-state current as a function of applied voltage offers a direct method to detect and characterize electron transfer processes in protein electrochemistry.[21] Combined with the STM, it provides high sensitivity in a quasibiological environment necessary for observing long-range charge transfer.[22,23] Similarly to tunneling junction experiments, in order to measure the single molecule conductivity a biomolecule is placed between the substrate and the tip. However, the sufficient stability, retention of the biological function and control of the molecular orientation at the interface still remain very challenging.[23] From the theoretical point of view, seeking stable biomimetic systems and understanding their fundamental properties are of great interest.

A considerable amount of work has been devoted to investigating inelastic tunneling in molecular junctions both theoretically[24–35] and experimentally.[36–40] In tunneling junctions, vibrations are associated with the inelastic scattering and energy dissipation leading to local heating effects. Experimentally, single molecule vibrations can be detected and characterized with the inelastic electron-tunneling spectroscopy (IETS).[36,41–43] Although mostly used to study simple organic molecules, recently the IETS has been successfully applied to the analysis of large protein polypeptides.[44] However, the analysis and interpretation of the IETS results for proteins are a serious theoretical challenge. Understanding how the atomic vibrations of various amino acids in a protein couple to the tunneling electrons is of particular interest and will be the principal focus of this paper.

We choose polypeptide bridges as the main subject of our study for the following reasons. First, polypeptides are the building blocks of more complex biological molecules (proteins). Though structurally simple, they retain some of the protein functions. Second, to measure conductance of a single molecule it has to interface with the macroscopic electrodes. In fact, one needs to contact the molecule from both ends in order to pass the current through. The β-sheet configuration of a polypeptide chain allows for such electrode-molecule interfacing. To study the charge transfer across a polypeptide bridge we sandwich it between two metal electrodes and apply external bias. There are at least two possible mechanisms for the electron to travel along the bridge: sequential hopping and tunneling. The transition between the hopping and tunneling regimes during the electron transfer has been discussed in the literature.[45,46] In this paper we shall consider the electron tunneling as the prime mechanism for charge transfer in protein bridges and focus on its steady-state interpretation.

In order to study inelastic scattering in polypeptides we employ density-functional theory (DFT) within the nonequilibrium Green's function (NEGF) formalism. With that we are able to calculate the tunneling current inside a polyanaline bridge. The NEGF-DFT method has been successfully applied in molecular electronics to study the charge transfer in molecular tunneling junctions.[33–35,47] It allows for a self-consistent calculation of the molecular Hamiltonian under the open boundary conditions and, if necessary, under the electron flow. By diagonalizing the dynamical matrix generated in such a calculation we compute the vibrational spectrum of the molecule (under bias). We include these vibrations self-consistently into the probability current calculation.[33,35] Our analysis of the inelastic electron tunneling in polyalanine shows that molecular vibrations substantially change the charge-transfer efficiency of the bridge.

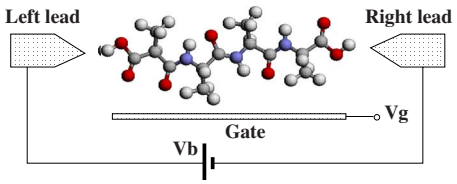

FIG. 1. (Color online) Schematic plot of the electrode-bridge-electrode system. In our approach the peptide molecular bridge is placed between two metal contacts. The bias voltage is then applied to the contacts in order to study its transport properties. The gate electrode is used to control the band alignment.

We would like to point out that in what follows we do not consider the effect of conformational changes in the protein bridge but only include the effect of small oscillations of the bridge atoms around their equilibrium positions. If the time scale of such fluctuations is comparable to the time of an electron staying on the molecular bridge, then an electron may gain or lose energy by absorbing or emitting phonons corresponding to vibrational modes of the bridge. We can roughly estimate the electron resonant lifetime τ as

$$\tau = \hbar/2\Delta\epsilon_m, \tag{1}$$

where $\hbar$ is the Planck's constant and $\Delta\epsilon_m$ is the half width of the resonant peak at its half maximum value around the energy ϵ_m, evaluated from the plot of the transmission coefficient versus energy (see Sec. III, for example). The electron resonant lifetime in the bridge is roughly $\approx 3\times 10^{-14}$ s or the same order as the period of characteristic molecular oscillations. Therefore, an electron will likely scatter by a phonon while traveling through the bridge. This results in additional electron-tunneling channels and modifies the probability current.

The rest of the paper is organized as follows. In Sec. II we explain the essential features of the theoretical formalism. In Sec. III we describe the electronic and vibrational properties of polyalanine bridges and discuss elastic transport. In Sec. IV we discuss the problem of alignment of the donor/acceptor states of the contact with the electronic states of the bridge. In Sec. V we present the results of our calculations of inelastic tunneling and analyze the vibrational modes strongly contributing to charge transfer. In Sec. VI we introduce a simple model illustrating our *ab initio* results. We conclude with a short summary.

II. THEORETICAL FORMALISM

As mentioned in the previous sections, we consider a molecule between two metallic electrodes, thus making it an electrode-bridge-electrode (EBE) system, as shown schematically in Fig. 1. Applying bias voltage across the EBE system makes electrons in the donor states of the left electrode tunnel through the bridge into the acceptor states of the right electrode so that the net tunneling current can be calculated.

The total Hamiltonian of the polypeptide EBE system including the interaction with the phonons has a general form[48,49]

$$\hat{H} = H_{\rm e} + \hat{H}_{\rm mv} + \hat{H}_{\rm e\text{-}mv}, \tag{2}$$

where $\hat{H}_{\rm e}$ is given by the Kohn-Sham (KS) Hamiltonian that describes explicitely the electronic states of the bridge coupled to the donor/acceptor states of the electrodes. We employ the local-density approximation,[50] norm-conserving pseudopotentials,[51,52] and local-orbital basis.[53] $\hat{H}_{\rm mv}$ is the Hamiltonian of the molecular vibrations in the bridge and within the second quantization it is given by

$$\hat{H}_{\rm mv} = \sum_n \hbar\omega_n \left(\hat{b}_n^+ \hat{b}_n + \frac{1}{2}\right). \tag{3}$$

Here $\hat{b}$ and $\hat{b}^+$ are the creation and anihilation operators of quantized molecular vibrational modes of the bridge. The electron-molecular vibration (e-mv) interaction Hamiltonian $\hat{H}_{\rm e\text{-}mv}$ can be written in the localized atomic orbital basis as

$$\hat{H}_{\rm e\text{-}mv} = \sum_n \sum_{\mu\nu} g_{\mu\nu}^n |\phi_\mu\rangle\langle\phi_\nu|(\hat{b}_n^+ + \hat{b}_n), \tag{4}$$

where the e-mv coupling matrix $g_{\mu\nu}^n$ is defined in the representation of the atomic-orbital basis functions $|\phi_\mu\rangle$ (μ is the orbital index) as

$$g_{\mu\nu}^n = \sum_K \sqrt{\frac{\hbar}{2M_K\omega_n}} \mathbf{e}_K^n \langle\phi_\mu| \frac{\partial \hat{H}_{\rm e}}{\mathbf{R}_K} |\phi_\nu\rangle. \tag{5}$$

The gradient is calculated at the equilibrium atomic positinos $\mathbf{R}_J = \mathbf{R}_J^0$. ω_n and $\mathbf{e}_K^n$ are the eigenfrequencies and eigenvectors of the dynamical matrix of the molecule, respectively. The electron-molecular vibration coupling matrix tells us how strongly the electron tunneling through the bridge is affected by the nuclear motion.

Once the electronic Hamiltonian is written, the self-consisted electron charge density is calculated. We compute the charge density as

$$\hat{\rho} = -\frac{1}{2\pi}\int dE G^<(E), \tag{6}$$

where the nonequilibrium Green's function is defined in terms of the retarded and advanced Green's functions,

$$G^{\gtrless}(E) = G^R(E)[\Sigma_L^{\gtrless}(E) + \Sigma_R^{\gtrless}(E) + \Sigma_{\rm e\text{-}mv}^{\gtrless}(E)]G^A(E). \tag{7}$$

Here $\Sigma_{L/R}^{\gtrless}(E)$ is the self-energy operator describing charge injection from the left/right electrode,[47] $\Sigma_{\rm e\text{-}mv}^{\gtrless}(E)$ is the self-energy describing e-mv interactions.[49]

At first we compute the electron density and KS Hamiltonian self-consistently within the NEGF-DFT. At this stage we do not include the e-mv interactions and the NEGF is obtained with $\Sigma_{\rm e\text{-}mv}^{\gtrless}(E)=0$. Provided with the total energy we compute the dynamical matrix [the second derivative of the energy $E(\{\mathbf{R}_i\})$ with respect to atomic positions $\{\mathbf{R}_i\}$] which we then diagonalize and obtain vibrational eigenfrequencies ω_n and eigenvectors $\mathbf{e}_n$ (n is the mode index). Then, the electron-molecular vibration coupling strength matrix g^n is calculated according to Eq. (5).

Having obtained the e-mv coupling matrix and the set of vibrational eigen modes, we include the effect of the e-mv

interaction using perturbation theory. The molecular vibrations then produce an effective potential which alters the electronic Hamiltonian while the electronic Green's functions are perturbed by the appropriate e-mv self-energies. We use the lowest-order Feynman diagrams to compute the e-mv self-energy[54] so that only the single-vibration processes are included. The vibrations within such perturbative approach need to be treated self-consistently. The role of self-consistency here is twofold. First, there is self-consistency between the Green's function and the e-mv self-energy.[33] Second, and in our opinion more importantly, self-consistency appears in the relationship between the electronic Hamiltonian and electron charge density. This second self-consistency is absolutely necessary for the inelastic tunneling because the e-mv coupling changes during the current flow and thus depends on the nonequilibrium physics.[34]

Once the iterative solution for the Hamiltonian and Green's functions is obtained, all relevant transport quantities such as the transmission coefficient and inelastic tunneling current can be calculated. In particular, the total transmission function can be written as a sum of elastic and inelastic components

$$T_{L/R} = T^{el}_{L/R} + T^{inel}_{L/R}, \tag{8}$$

where the elastic transmission is obtained from the Green's functions via the Fisher-Lee relationship,[55]

$$T^{el}_{L/R} = \mathrm{Tr}[\Gamma_{L/R} G^R \Gamma_{R/L} G^A]. \tag{9}$$

The inelastic transmission function is written in a similar manner

$$T^{inel}_{L/R} = \mathrm{Tr}[\Gamma_{L/R} G^R \Gamma_{\text{e-mv},R/L} G^A], \tag{10}$$

here $\Gamma_{\text{e-mv}}=\Gamma_{\text{e-mv},L}+\Gamma_{\text{e-mv},R}$ is the linewidth function due to e-mv interactions and $\Gamma_{L/R}$ are linewidth functions describing coupling between the bridge and donor/acceptor centers. They can be written in terms of the appropriate self-energies respectively as

$$\Gamma_{\text{e-mv},L/R} = i[\Sigma^{>}_{\text{e-mv},L/R}(E) - \Sigma^{<}_{\text{e-mv},L/R}(E)] \tag{11}$$

and

$$\Gamma_{L/R} = i[\Sigma^{>}_{L/R}(E) - \Sigma^{<}_{L/R}(E)]. \tag{12}$$

When no phonons are present in the system, an electron may tunnel elastically so that the initial and final energies are the same. In the presence of the e-mv interaction, an electron can still tunnel elastically but may also be involved in a virtual de-excitation and excitation of the vibrational quantum while effectively keeping the same energy. In addition, an electron may emit or absorb phonons which creates extra, inelastic, tunneling channels. The details of our inelastic NEGF-DFT formalism can be found in Ref. 49.

III. POLYALANINE BRIDGE AND ELASTIC CHARGE TRANSFER

To perform atomic simulations for the dipeptide, tripeptide, and quartopeptide chains with the number of peptide bonds varying from 1 to 3 we place a polypeptide bridge terminated with carboxyl termini and with the alanine acid CH_3 as an amino group between two Al(100) electrodes, as shown in Fig. 1. Each lead has four layers of Al atoms in the transport direction. No constraints are applied to the positions of the atoms unless stated otherwise.

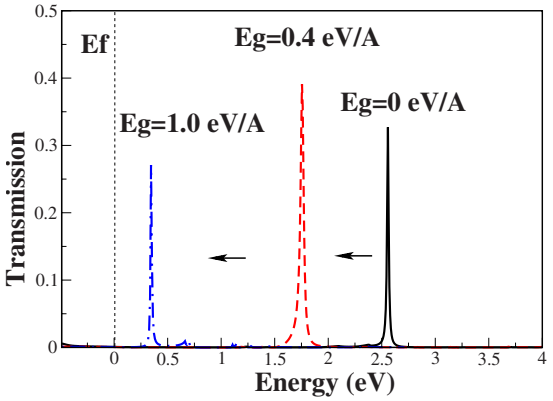

FIG. 2. (Color online) The transmission versus electron-tunneling energy for the dialanine bridge (no e-mv interaction included) at different values of the applied gate electric field. Increasing the value of the gate potential shifts the LUMO level of the polypeptide bridge toward the Fermi energy of the tunneling junction. The Fermi level is set to $E=0$ eV.

The polyalanine bridges are in the β-sheet conformation rather than α-helix one since they are too short to form a helix. To obtain stable geometry of the bridge a total-energy relaxation within NEGF-DFT framework is carried out. We first perform DFT calculations of an isolated alanine dipeptide molecule and find the gap between the highest occupied molecular orbital (HOMO) and lowest unoccupied molecular orbital (LUMO) to be about 3.5 eV. When connected to Al leads the HOMO-LUMO gap remains the same, the Fermi level of the leads is 1 eV above the HOMO. The calculated transmission coefficient as a function of the electron-tunneling energy for the dialanine bridge with no e-mv interaction included is shown in Fig. 2. The transmission resolves several sharp peaks. To understand their origin we examine molecular orbitals of the polypeptide bridge interacting with the leads by diagonalizing the submatrix corresponding to the bridge inside the full DFT Hamiltonian. In the following, we refer to these orbitals as "renormalized molecular orbitals" (RMOs). The energies of the RMOs align well with the position of the transmission peaks indicating that the electron charge transfer in polyalanine bridges is resonant in nature. The electron tunnels through when the Fermi level of the leads aligns with molecular states. The sharpness of the peaks confirms the weak coupling to the leads.

In addition we calculate the vibrational spectrum of the alanine bridge coupled to the leads. In particular, for dialanine we find 66 vibrational modes with frequencies ranging from 130 to 3000 cm^{-1}. As a check we also perform phonon spectrum calculations for an isolated dipeptide molecule and obtain the frequencies in the same range indicating that the phonons are not altered significantly by the leads.

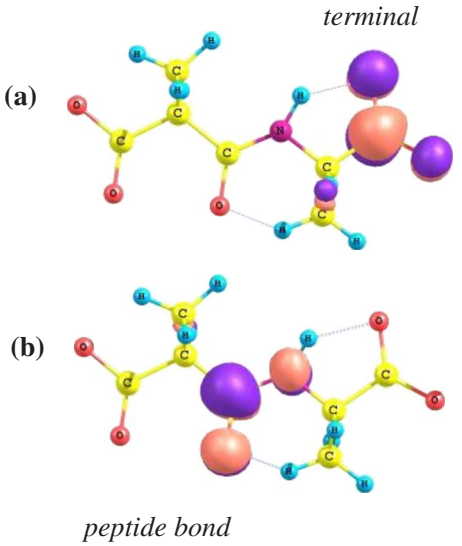

FIG. 3. (Color online) Spatial distribution plot of several low-lying LUMO-derived RMOs for the dialanine bridge. (a) Two orbitals are localized on the carboxyl group and (b) one on the peptide bond.

IV. BAND ALIGNMENT: ENHANCED CHARGE INJECTION

We find that a large HOMO-LUMO gap makes electron charge transfer in the bridge almost impossible. Indeed, a bias of at least 2.5 eV is needed for the electron jump to the LUMO-derived orbital. Large bias voltages in DFT sometimes create divergence in the self-consistent procedure and may lead to nonphysical results. Alternatively, one can use a different electrode with the Fermi level better aligned with the molecular levels. However, the simplicity of Al makes it attractive from the computational point of view. We apply a positive voltage to the gate electrode (schematically shown in Fig. 1) so that the energy gap between the Fermi energy and the LUMO can be controlled. Indeed, the applied gate potential produces the electric field which shifts molecular states down. Consequently, the transmission peaks related to the LUMO-derived orbital moves toward the Fermi level, as shown in Fig. 2. A similar behavior is observed for trialanine and quartoalanine bridges; applying an electric field of about 1 V/Å facilitates the charge transfer through the LUMO-derived states.

In Fig. 3 we plot the spatial distribution of several low-lying RMOs above the Fermi energy that are responsible for the charge transfer through the polypeptide. For dialanine there are two RMOs localized on the carboxyl group having lowest and relatively close energies, and one localized on the peptide bond of the bridge. In the following, we refer to the first two orbitals as the carboxyl-LUMOs and to the other as the peptide-LUMO. To understand which of these molecular orbitals plays a significant role in the charge-transfer mechanism we project scattering states across the bridge, contributing to the transmission peaks shown in Fig. 2, onto RMOs at zero gate bias,

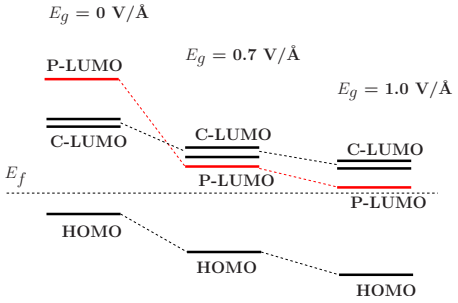

FIG. 4. (Color online) Schematic plot of several molecular orbitals of the dialanine bridge at different value of the gate electric field E_g. The LUMO-derived orbitals localized on the carboxyl termini and the peptide bond are labeled as C-LUMO and P-LUMO, respectively. Clearly, at $E_g \approx 0.7$ eV/Å these orbitals switch order, hence making the electron tunnel through the peptide-LUMO state.

$$\hat{P}_{\mathrm{RMO}}\Psi_{sc}(\epsilon,k) = \sum_i a_i(\epsilon,k)|\mathrm{RMO}_i\rangle, \tag{13}$$

where $\Psi_{sc}(\epsilon,k)$ is the scattering state across the bridge and summation is over the target RMOs. Note that the scattering states describe electron-tunneling channels and our technique allows us to analyze each of them individually. We find that for dialanine only the peptide-LUMO state contributes to the charge transfer across the bridge while carboxyl-LUMOs do not play any role. A similar behavior is observed for the trialanine and quartoalanine bridges. The only difference is in the number of orbitals localized on the peptide bonds, two RMOs for trialanine and three for quartoalanine. Importantly, when the electric potential is applied to the gate electrode the carboxyl- and peptide-LUMOs are not shifted down in energy equally. In fact, we find that at the gate field of $E_g \approx 0.7$ V/Å, these states switch order in energy. Figure 4 shows a schematic plot of relevant molecular orbitals of dialanine at different gate voltages. Other molecular orbitals are significantly higher in energy than the carboxyl- and peptide-LUMOs, and thus do not directly contribute to the charge transfer. Indeed, the next state to the carboxyl-LUMOs is separated by ≈1.7 eV and is unreachable within the bias window used.

V. PHONON-ASSISTED CHARGE TRANSFER

Until now we have described the charge transfer in polyalanine bridges with no e-mv interactions. To answer how molecular vibrations change the electron transfer rate we include the e-mv coupling terms into the Hamiltonian and Green's functions following the self-consistent procedure discussed earlier.

In Fig. 5 we plot the total transmission function of dialanine under applied gate electric field of 1.0 V/Å in the presence of e-mv interaction calculated using Eqs. (9) and (10). We find that, in the presence of the e-mv interactions, the main transmission peak (originated from the resonance-mediated tunneling through the peptide-LUMO state) is diminished. The transmission function plot reveals several other peaks mainly due to the inelastic channels. We observe a single peak near the Fermi energy of the leads and a set of

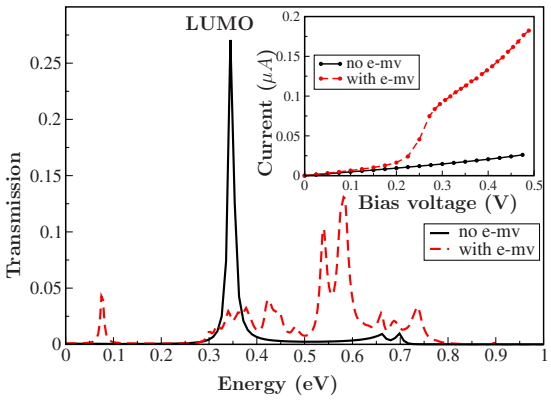

FIG. 5. (Color online) Total transmission function versus energy for the dialanine bridge with no e-mv coupling (solid line) plotted for comparison with that of e-mv coupling (dashed line). When the e-mv interaction is taken into account, main sharp transmission peak is splitted and contributed by the side-band peaks resulted from the tunneling through the inelastic channels. The origin of such splitting is discussed in the next section. Inset: the tunneling current with no e-mv coupling (solid line) and with e-mv coupling (dashed line). The Fermi energy is shifted to zero.

peaks from 0.3 to 0.8 eV above the Fermi energy. The total current, computed by integrating the transmission over the transport energy window, is drastically enhanced by the e-mv coupling, as shown in the inset of Fig. 5.

It is useful to plot the elastic and inelastic components of the transmission function separately [see Figs. 6(a) and 6(b), respectively]. The elastic part of transmission shows the splitting of the main peak. The inelastic component resolves many additional peaks assigned to appropriate vibrational modes. Such assignment is far from being straightforward: the positions of these peaks do not match the frequencies of

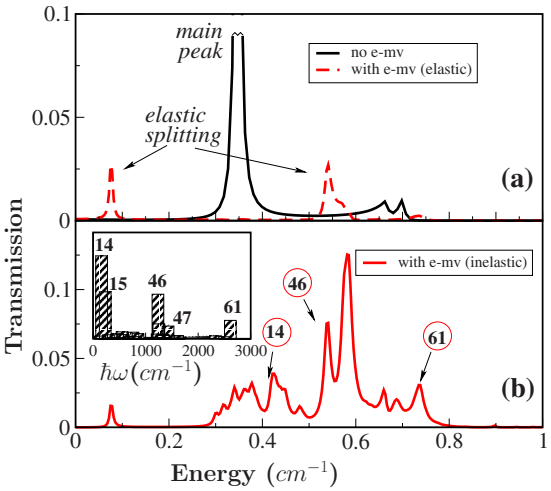

FIG. 6. (Color online) (a) Comparison of the transmission function with no e-mv interaction with the elastic component of that with the e-mv interaction at the gate electric field $E_g \approx 1.0$ V/Å and (b) the inelastic component of the transmission function with the e-mv interaction showing some distinct peaks resulted from the e-mv coupling with the vibrational modes 14, 46, and 61. The inset shows the e-mv coupling strength versus the frequency of the vibrational modes computed via Eq. (14).

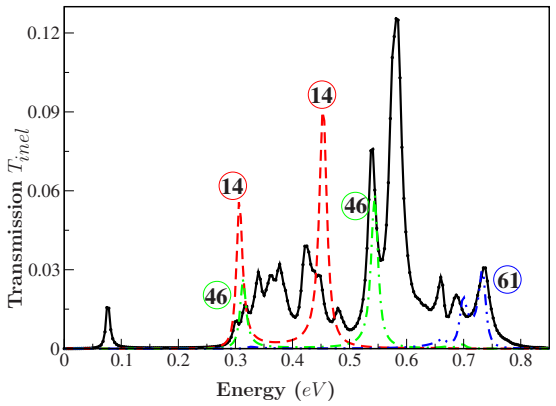

FIG. 7. (Color online) The inelastic component of the transmission function versus energy for dialanine bridge at the applied gate field E_g=1.0 V/Å. The transmission function with all vibrational modes included in the calculation (solid line) is to be compared with ones when only one of them [modes 14 (dashed line), 46 (dotted-dashed line), and 61 (double dotted-dashed line)] is included.

the bridge vibrational modes. Some of the peaks are even out the energy range of the vibrational spectrum. We estimate how strongly the electrons of the LUMO-derived states are coupled with the bridge vibrations by calculating the e-mv coupling strength for these states defined as

$$\lambda^n \equiv \frac{\langle \mathrm{LUMO}|g^n|\mathrm{LUMO}\rangle}{\hbar\omega_n}, \tag{14}$$

where g^n is the e-mv coupling matrix and LUMO is the LUMO-derived orbital localized on the peptide bond of the bridge that mediates the charge transfer. The inset in Fig. 6 shows the e-mv coupling strength for this orbital versus the phonon frequency. Clearly, there are a few modes out of total 66 that couple far stronger than the others. These include modes 14, 15, 46, and 61 with the frequencies 163, 231, 1250, and 2613 cm^{-1}, respectively. We find that the eigenvectors of these modes are localized on the peptide bonds.

Next, we perform three self-consistent calculations, each including only one of these three vibrational modes of interest and excluding all other modes. Having obtained the self-consistency between the inelastic electronic Hamiltonian and the Green's functions, we compute the transmission function and plot its inelastic component in Fig. 7. For comparison, the transmission obtained from the calculation that include all the vibrational modes is also shown. Comparing the inelastic transmission with all modes included with ones when only a single mode is included we conclude that the sharp peaks mostly originate from the inelastic tunneling through the channels created by the molecular vibrations with strong electron-phonon coupling. The difference in amplitude of these transmission peaks may results from the mutual influence of various vibrational modes included in the calculations through the electron density in our self-consistent calculations. Note that other vibrational modes, such as 14 and 46, also show strong e-mv coupling (see the inset of Fig. 6). However, for the sake of simplicity and clarity of Fig. 7 we

do not show the inelastic transmission curves related to these modes.

At this point of our analysis, the features of the inelastic transmission are associated with the particular vibrational modes with strong coupling. However, there are several fundamental questions that remain unclear. Why do we observe the splitting of the main transmission peak? Why does a single vibrational mode contribute to the elastic transmission function as a double-peak structure? What is the relation of the vibrational mode frequency and its e-mv coupling strength with the peak's splitting? It is rather difficult to answer these questions within the complete NEGF-DFT picture. In the next section we discuss a simple model, with just one electronic level and one phonon mode, that captures the essential physics of our calculations.

VI. A SIMPLE ONE-LEVEL MODEL WITH A SINGLE PHONON MODE

Consider a "molecule" with a single electron level with the energy E_0 interacting with two electrodes and one vibrational mode with the frequency ω. The total Hamiltonian can be written as[54]

$$\hat{H} = E_0\hat{d}^+\hat{d} + \sum_{k\alpha} \epsilon_k \hat{c}^+_{k\alpha}\hat{c}_{k\alpha} + \sum_{k\alpha} T_{k\alpha}(\hat{c}^+_{k\alpha}\hat{d} + \text{c.c.}) + \hbar\omega\left(\hat{b}^+\hat{b} + \frac{1}{2}\right) + g\hat{d}^+\hat{d}(\hat{b}^+ + \hat{b}). \tag{15}$$

In the above model $\epsilon_{k\alpha}$ is the energy of conduction electrons in the α electrode ($\alpha=L$ and R for left and right) and is characterized by the wave vector $\mathbf{k}$. The operator $\hat{c}^+_{k\alpha}(\hat{c}_{k\alpha})$ creates (annihilates) a conduction electron inside the α electrode. Similarly, $\hat{d}^+(\hat{d})$ is the creation (annihilation) operator of electrons for the molecule region. $T_{k\alpha}$ describes the coupling of the molecule to the α electrode. The operator $\hat{b}^+(\hat{b})$ creates (annihilates) a phonon inside the molecule and g is the e-mv coupling function. Using the equation of motion method[54] we obtain the analytical expression for the retarded Green's function,

$$G^R = [E - E_0 - \Sigma^R_L - \Sigma^R_R - \Sigma^R_{\text{e-mv}}]^{-1}, \tag{16}$$

where $\Sigma^R_{L/R}$ is the retarded self-energy describing the interaction with the left/right electrode and $\Sigma^R_{\text{e-mv}}$ is the retarded self-energy of the e-mv interaction.

To simplify our calculation even further we approximate the self-energies of the electrodes and of the e-mv interaction in Eq. (16) as[56]

$$\Sigma^R_{L/R} = -\imath\frac{1}{2}\Gamma_{L/R} \tag{17}$$

and

$$\Sigma_{\text{e-mv}}(E) = gG^R_0(E - \hbar\omega)g, \tag{18}$$

respectively. Here $G^R_0(E)$ is the retarded Green's function with no electron-phonon interaction included and $\Gamma_{L/R}$ is the linewidth function for the left/right electrode which in a wide-band limit is given by[56]

$$\Gamma_\alpha(\epsilon) = 2\pi\sum_k |T_{k\alpha}|^2\delta(\epsilon - \epsilon_{k\alpha}). \tag{19}$$

Within this approximation, the retarded Green's function takes the form

$$G^R = \left\{E - E_0 + \imath\frac{1}{2}(\Gamma_L + \Gamma_R) - g^2\left[E - E_0 - \hbar\omega + \imath\frac{1}{2}(\Gamma_L + \Gamma_R)\right]^{-1}\right\}^{-1}. \tag{20}$$

Now both elastic and inelastic components of the transmission function can be easily obtained via Eqs. (9) and (10), respectively. In the previous section we have learnt that vibrational modes with different frequencies and e-mv coupling strength contribute differently to the total tunneling. For instance, mode 13 shows a two-peak contribution while mode 62 results in just a single peak. The reason lies in the mutual relationship between the e-mv coupling strength and the frequency of the particular vibrational mode. Let us consider three possible situations: (i) e-mv coupling g is greater than the vibrational energy $\hbar\omega$, (ii) the energy $\hbar\omega$ is greater than the e-mv coupling g, and (iii) the energy $\hbar\omega$ is greater than the e-mv coupling and at the same time greater than the energy of the molecular level E_0 (in fact E_0-E_f but for the sake of simplicity, the Fermi energy E_f is set to zero).

With the help of Eq. (20) we can analyze both elastic and inelastic transmissions. For example, taking the derivative of the elastic component of the transmission function over the energy in the limit $\Gamma_{L/R}=0$ we find that it has two maxima characterized by the energies

$$E = E_0 + \frac{\hbar\omega}{2} \pm \frac{1}{2}\sqrt{\hbar\omega^2 + 4g^2}. \tag{21}$$

Note that the limit $\Gamma_{L/R}=0$ is not necessary but is used to simplify Eq. (21).

One can consider three limiting cases. (i) When the e-mv coupling g is much greater that the vibrational energy $\hbar\omega$, the above expression is approximated by

$$E \approx E_0 + \frac{\hbar\omega}{2} \pm \left(g + \frac{1}{2\sqrt{2}}\frac{\hbar\omega}{g}\right). \tag{22}$$

Clearly, in the limit $\hbar\omega=0$, the retarded Green's function and the transmission functions have the maxima at $E\approx E_0\pm g$.

(ii) When $\hbar\omega \gg g$, Eq. (21) is rewritten as

$$E \approx E_0 + \frac{\hbar\omega}{2} \pm \left(\frac{\hbar\omega}{2} + \frac{g}{\hbar\omega}\right). \tag{23}$$

If the e-mv coupling g is negligibly small, then the transmission functions are expected to have two maxima at the energies $E\approx E_0$ and $E\approx E_0+\hbar\omega$. Note that in this model, the e-mv coupling g is never zero; otherwise the inelastic term of the retarded Green's function in Eq. (20) vanishes and the scattering problem becomes purely elastic.

(iii) Furthermore, the inelastic contribution to the transmission [see Eq. (10)] includes the Fermi distribution function $f(E_0-\hbar\omega)$ (see Ref. 49). Therefore when the vibrational energy $\hbar\omega$ becomes greater than the electron energy E_0, the

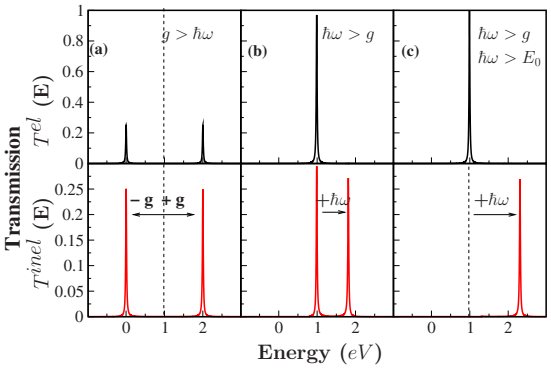

FIG. 8. (Color online) Elastic and inelastic transmission functions versus energy for the one-level model at different values of e-mv coupling g and vibrational energy $\hbar\omega$: (a) $g > \hbar\omega$, (b) $\hbar\omega > g$, and (c) $\hbar\omega > g$ and $\hbar\omega > E_0$. The Fermi energy is set to zero.

maximum of the transmission function at $E=E_0$ vanishes. The physics behind this effect is as follows: an electron tunnels inelastically only when its energy reaches the threshold of the excitation of the vibrational mode.

Figure 8 shows the elastic and inelastic transmission functions versus electron energy for different values of the e-mv coupling g and vibrational energy $\hbar\omega$. In the following we use fixed electrode linewidth functions $\Gamma_{L/R}=0.03$ eV. The e-mv coupling g is chosen to be always greater than the electrode linewidth functions so that the system is in the resonant regime $(g \gg \Gamma_L+\Gamma_R)$.

We start by setting the e-mv coupling g to be greater than the vibrational energy ($g=1.0$ eV and $\hbar\omega=0.1$ eV). When no e-mv interaction present in the system, we expect just a single transmission peak at $E=E_0$. However, when the e-mv coupling is included, we observe that both elastic and inelastic transmission functions resolve two peaks at the energies $\approx E_0 \pm g$ [see Fig. 8(a)]. In this limit the noninteracting peak splits into two satellite peaks. This observation suggests that the electronic energy level is strongly perturbed by the e-mv interaction which leads to new resonant levels.

When the vibrational energy $\hbar\omega$ is greater than the e-mv coupling g ($\hbar\omega=0.8$ eV and $g=0.1$ eV) we find that elastic transmission functions has a single peak at the energy $E \approx E_0$ while the inelastic function plot resolves two peaks at the energies $E \approx E_0$ and $E \approx E_0+\hbar\omega$, shown in Fig. 8(b). This is what one would expect from perturbation theory. The electron has an extra channel to tunnel through the system inelastically by emitting the phonon with the energy $\hbar\omega$. Further increasing the vibrational energy $\hbar\omega$ up to 1.3 eV makes the peak in the inelastic transmission function plot at the energy $E \approx E_0$ vanish, as shown in Fig. 8(c).

We can now explain the behavior of the dialanine transmission function presented in the previous section (see Fig. 7). For example, modes 14 and 15 have a relatively strong e-mv coupling strength, as shown in the inset of Fig. 7 and small vibrational frequency (162 and 231 cm^{-1}, respectively). Therefore, each of these modes contributes with two peaks to the inelastic transmission function, essentially renormalizing the electronic state. We shall call these type I modes. On the other hand, mode 61 is described by the small e-mv coupling and large phonon frequency, thus producing a single peak in the inelastic transmission. This is the type II mode.

Since in most cases long-range charge transfer has to be resonance mediated this picture can be generalized. The resonance tunneling is dominated by a particular set of molecular orbitals. Once the relevant orbitals are identified their coupling to the molecular vibrations can be evaluated. Depending on whether the frequency of the strongly coupled vibration is high or low, its contribution to the inelastic charge transfer can be of two types. If the frequency is high, two usual symmetric side bands will appear. However, the low-frequency modes will cause the split proportional to the e-mv coupling rather than frequency. Another observation is that high-frequency modes correspond to strong sigma bonding and thus are more likely to couple with high energy electronic states irrelevant to "low-bias" charge transfer.

In conclusion, we investigate the charge transfer through short alanine bridges using the NEGF-DFT formalism and study the effect of molecular vibrations on tunneling. We find that the electron tunneling is resonant in nature and mediated by molecular states of the molecular bridge localized on peptide bonds. The inelastic processes due to molecular vibrations significantly increase the efficiency of charge transfer. With the help of a simplified model we show that depending on the frequency of molecular vibrations the inelastic scattering could fall into two different tunneling regimes. Based on a detailed analysis of the dialanine molecule we argue that, in general, the effect of low-frequency vibrational modes in charge transfer is more pronounced.

ACKNOWLEDGMENTS

We thank Qian Niu for insightful discussions and P. Rossky and D. Makarov for reading the manuscript. This work is supported by the Welch Foundation under Grant No. F-1624.

*demkov@physics.utexas.edu

[1] A. Aviram and M. Ratner, Chem. Phys. Lett. **29**, 277 (1974).
[2] J. Chen, M. Reed, A. Rawlett, and J. Tour, Science **286**, 1550 (1999).
[3] C. Collier, Science **285**, 391 (1999).
[4] R. Metzger, Chem. Rev. (Washington, D.C.) **103**, 3803 (2003).
[5] M. Reed, J. Chen, A. Rawlett, D. Price, and J. Tour, Appl. Phys. Lett. **78**, 3735 (2001).
[6] Z. Keane, J. Ciszek, J. Tour, and D. Natelson, Nano Lett. **6**, 1518 (2006).
[7] H. Wang, S. Lin, J. Allen, J. Williams, S. Blankert, C. Laser, and N. Woodbury, Science **316**, 747 (2007).
[8] S. Skourtis and D. Beratan, Science **316**, 703 (2007).
[9] S. Franzen, L. Kiger, C. Poyart, and J.-L. Martin, Biophys. J. **80**,

2372 (2001).
[10] V. Novoderezhkin, J. Dekker, and R. van Grondelle, Biophys. J. **93**, 1293 (2007).
[11] K. Krab and M. Wikstrom, Biochim. Biophys. Acta **895**, 25 (1987).
[12] S. Flores and V. Batista, J. Phys. Chem. B **108**, 6745 (2004).
[13] M. Reed, C. Zhou, C. Muller, T. Burgin, and J. Tour, Science **278**, 252 (1997).
[14] D. Porath, A. Bezryadin, S. de Vries, and C. Dekker, Nature (London) **403**, 635 (2000).
[15] M. Dorogi, J. Gomez, R. Osifchin, R. P. Andres, and R. Reifenberger, Phys. Rev. B **52**, 9071 (1995).
[16] R. Andres, T. Bein, M. Dorogi, S. Feng, J. Henderson, C. Kubiak, W. Mahoney, R. Osifchin, and R. Reifenberger, Science **272**, 1323 (1996).
[17] X. Xiao, B. Xu, and N. Tao, Nano Lett. **4**, 267 (2004).
[18] S. Sek, K. Swiatek, and A. Misicka, J. Phys. Chem. B **109**, 23121 (2005).
[19] X. Xiao, B. Xu, and N. Tao, J. Am. Chem. Soc. **126**, 5370 (2004).
[20] X. Xiao, B. Xu, and N. Tao, Angew. Chem., Int. Ed. **43**, 6148 (2004).
[21] A. Mechler, G. Nawaratna, M.-I. Aguilar, and L. Martin, International Journal of Peptide Research and Therapeutics **12**, 217 (2006).
[22] J. Zhang, Q. Chi, A. Kuznetsov, A. Hansen, H. Wackberbath, H. Christensen, J. Andersen, and J. Ulstrup, J. Phys. Chem. B **106**, 1131 (2002).
[23] Q. Chi, O. Farver, and J. Ulstrup, Proc. Natl. Acad. Sci. U.S.A. **102**, 16203 (2005).
[24] Y.-C. Chen and M. Di Ventra, Phys. Rev. Lett. **95**, 166802 (2005).
[25] Y.-C. Chen, M. Zwolak, and M. D. Ventra, Nano Lett. **4**, 1709 (2004).
[26] Y.-C. Chen, M. Zwolak, and M. D. Ventra, Nano Lett. **3**, 1691 (2003).
[27] A. Pecchia, A. D. Carlo, A. Gagliardi, T. Niehaus, and T. Frauenheim, J. Comput. Electron. **4**, 79 (2005).
[28] A. Pecchia, G. Romano, and A. Di Carlo, Phys. Rev. B **75**, 035401 (2007).
[29] M. Galperin, M. Ratner, and A. Nitzan, J. Phys.: Condens. Matter **19**, 103201 (2007).
[30] G. Romano, A. Pecchia, and A. D. Carlo, J. Phys.: Condens. Matter **19**, 215207 (2007).
[31] A. Troisi and M. Ratner, J. Chem. Phys. **125**, 214709 (2006).
[32] U. Harbola, J. Maddox, and S. Mukamel, Phys. Rev. B **73**, 205404 (2006).
[33] T. Frederiksen, M. Brandbyge, N. Lorente, and A.-P. Jauho, Phys. Rev. Lett. **93**, 256601 (2004).
[34] N. Sergueev, D. Roubtsov, and H. Guo, Phys. Rev. Lett. **95**, 146803 (2005).
[35] N. Sergueev, A. A. Demkov, and H. Guo, Phys. Rev. B **75**, 233418 (2007).
[36] W. Ho, J. Chem. Phys. **117**, 11033 (2002).
[37] W. Wang, T. Lee, I. Kretzshmar, and M. Reed, Nano Lett. **4**, 643 (2004).
[38] J. Pascual, J. Gomez-Herrero, D. Sanchez-Portal, and H.-P. Rust, J. Chem. Phys. **117**, 9531 (2002).
[39] J. Pascual, N. Lorente, Z. Song, H. Conrad, and H.-P. Rust, Nature (London) **423**, 525 (2003).
[40] N. Pradhan, N. Liu, and W. Ho, J. Phys. Chem. **109**, 8513 (2005).
[41] D. Cass, H. Strauss, and P. Hansma, Science **192**, 1128 (1976).
[42] B. Stipe, M. Rezaei, and W. Ho, Science **280**, 1732 (1998).
[43] S. Khanna and J. Lambe, Science **220**, 1345 (1983).
[44] A. Luchini, D. Long, I. Vaisman, E. Petricoin, D. Geho, and L. Liotta, Res. Lett. Nanotech. **2008**, 853253 (2008).
[45] E. Medvedev and A. Stuchebrukhov, J. Chem. Phys. **107**, 3821 (1997).
[46] A. Felts, W. Pollard, and R. Friesner, J. Phys. Chem. **99**, 2929 (1995).
[47] J. Taylor, H. Guo, and J. Wang, Phys. Rev. B **63**, 121104(R) (2001).
[48] M. Galperin and M. Ratner, J. Chem. Phys. **121**, 11965 (2004).
[49] N. Sergueev, Ph.D. thesis, McGill University, 2005.
[50] J. P. Perdew and A. Zunger, Phys. Rev. B **23**, 5048 (1981).
[51] S. Goedecker, M. Teter, and J. Hutter, Phys. Rev. B **54**, 1703 (1996).
[52] D. R. Hamann, M. Schluter, and C. Chiang, Phys. Rev. Lett. **43**, 1494 (1979).
[53] S. Itoh, P. Ordejon, D. A. Drabold, and R. M. Martin, Phys. Rev. B **53**, 2132 (1996).
[54] A. Abrikosov, L. Gorkov, and J. Dzialoshinskii, *Quantum Field Theory in Statistical Physics* (Prentice-Hall, New York, 1963).
[55] D. S. Fisher and P. A. Lee, Phys. Rev. B **23**, 6851 (1981).
[56] S. Datta, *Electronic Transport in Mesoscopic Systems* (Cambridge University Press, Cambridge, England, 1997).